

# Frankenstein: Generating Semantic-Compositional 3D Scenes in One Tri-Plane

Han Yan<sup>1</sup>\*, Yang Li<sup>4</sup>, Zhennan Wu<sup>2</sup>, Shenzhou Chen<sup>4</sup>, Weixuan Sun<sup>4</sup>,  
Taizhang Shang<sup>4</sup>, Weizhe Liu<sup>4</sup>, Tian Chen<sup>4</sup>, Xiang Dai<sup>4</sup>, Chao Ma<sup>1</sup>,  
Hongdong Li<sup>3</sup>, and Pan Ji<sup>4</sup>

<sup>1</sup> Shanghai Jiao Tong University

<sup>2</sup> The University of Tokyo

<sup>3</sup> Australian National University

<sup>4</sup> Tencent XR Vision Labs

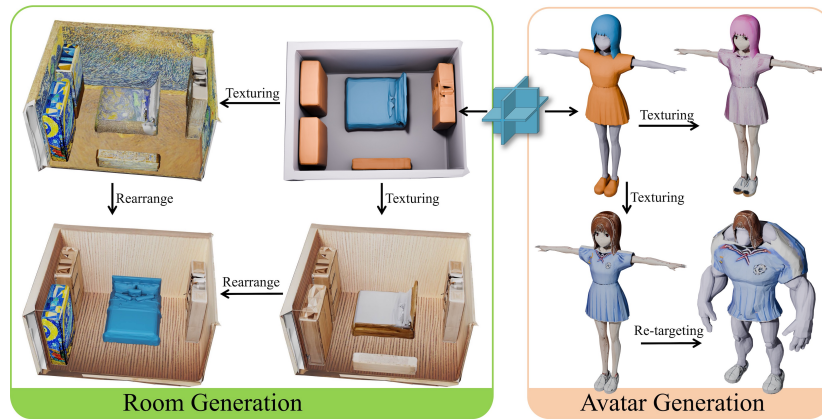


**Fig. 1:** We present Frankenstein, a tri-plane diffusion-based framework that can generate semantic-compositional 3D scenes in a single forward pass, e.g., rooms (left) and avatars (right). The generated scenes enable customized controls, such as part-wise texturing, and room object rearrangement or avatar cloth re-targeting.

**Abstract.** We present Frankenstein, a diffusion-based framework that can generate semantic-compositional 3D scenes in a single pass. Unlike existing methods that output a single, unified 3D shape, Frankenstein simultaneously generates multiple separated shapes, each corresponding to a semantically meaningful part. The 3D scene information is encoded in one single tri-plane tensor, from which multiple Signed Distance Function (SDF) fields can be decoded to represent the compositional shapes. During training, an auto-encoder compresses tri-planes into a latent space, and then the denoising diffusion process is employed to approximate the distribution of the compositional scenes. Frankenstein

\* The contribution of Han Yan and Zhennan Wu was made during an internship at Tencent XR Vision Labs.

demonstrates promising results in generating room interiors as well as human avatars with automatically separated parts. The generated scenes facilitate many downstream applications, such as part-wise re-texturing, object rearrangement in the room or avatar cloth re-targeting. The video is available on <https://youtu.be/1Rn-HqyCrLI>.

**Keywords:** 3D Scene Generation · Semantic Composition · Diffusion Model

## 1 Introduction

The creation of 3D assets with high-quality geometry is essential for many computer vision and graphics applications, including video gaming, film production and AR/VR. The progress in the denoising diffusion models [24] and Transformers [26] has significantly accelerated the development of 3D generative models. Recent works, such as [4, 10, 11, 20, 22], have demonstrated promising results on 3D assets generation using denoising diffusion. These methods typically generate 3D data in the form of a single neural field, such as a Neural Radiance Field (NeRF) [16] or a Signed Distance Function (SDF). Consequently, the generated 3D assets are entangled such that triangle meshes are not semantically distinguishable.

However, downstream applications often require semantically-decomposed 3D shapes. For example, in video games, a generated vehicle model should be able to be decomposed into a main body and its four roll-able wheels. Similarly, a 3D digital avatar shall be able to segment into parts like body, limbs, hair and apparel for realistic performance synthesis. Although semantic 3D segmentation tools may be applied to segment a mesh into meaningful parts, so far the performance of existing methods is far from satisfactory, sometimes leading to incomplete fragments. In this paper, we aim to develop a 3D generative AI model which enables directly generating semantic-compositional 3D scenes where each component has a complete shape.

Generating semantic-compositional 3D scenes poses two major challenges: Firstly, 1) a versatile 3D representation is required to jointly model the complete shape of multiple semantic components. Secondly, 2) modeling the relationships between different semantic parts is complex. The relative positions between various parts should be semantically meaningful and physically plausible, e.g., avoiding interpenetration.

To address these challenges, we present **Frankenstein**, a tri-plane diffusion-based approach that generates semantic-compositional 3D scenes. The tri-plane is a tensor used to factorize the dense 3D volume grid, which is followed by an MLP to decode the 3D neural field signal. We extend the tri-plane to represent compositional shapes by decoding multiple SDFs from a single tri-plane where each SDF contains the shape of a semantic class. This representation allows simultaneous modeling of multiple complete shapes inside a single tri-plane tensor. The training of Frankenstein consists of 3 stages: First, 1) through per-scene fitting, we convert training scenes into tri-planes, which implicitly encode

both the compositional shape information and the spatial relationships between components. Then, 2) a variational auto-encoder (VAE) is trained to compress tri-planes into a latent tri-plane space which is significantly more compact and computationally efficient. Lastly, 3) a denoising diffusion model is trained to approximate the distribution of the latent tri-planes. We evaluate Frankenstein for two types of scenes: rooms composed of different classes of furniture; and avatars with clothing, hair, and body parts. Frankenstein generates meaningful compositional scenes, ensuring a clear distinction between scenes, and also showcases diversity in the shapes it generates. The generated scenes facilitate downstream applications, including part-wise texturing, object rearrangement in the room, or avatar cloth re-targeting.

To summarize, our contributions are threefold:

- We propose the first 3D diffusion model that can generate semantic compositional scenes in one tri-plane with a single forward pass.
- We develop a robust coarse-to-fine optimization approach to produce high-fidelity semantic-compositional tri-planes.
- We demonstrate the capabilities of our method for generating both room scenes and compositional avatars.

## 2 Related Work

**3D Generation.** With the great success of diffusion model [24] in 2D domain [12, 21], numerous studies have started investigating how to build 3D generation models. There are mainly two technical solutions. One solution obtains 3D assets by distilling knowledge from pretrained 2D generator [19, 20]. DreamFusion [19] proposed Score distillation Sampling (SDS) to optimize a NeRF model with images generated by a 2D generator. Magic3D [20] utilized a coarse-to-fine two-stage strategy to improve both speed and quality. However, these methods usually suffer from the multi-view inconsistency problem and require time-consuming optimization. The other technical solution involves directly training 3D generators using ground truth 3D data. Rodin [27] collected 100K 3D avatars using a professional synthetic engine and trained 3D-aware tri-plane diffusion model to generate NeRF [16] of the avatars. Similar tri-plane diffusion-based methods can be found in [11, 23]. LAS [34] instead directly performed diffusion on the 3D voxel grid. LRM [14] formulated 3D generation as a deterministic 2D-to-3D reconstruction problem. This paper builds upon the concept of tri-plane diffusion but introduces a major change: we encode multiple signed distance functions into a single tri-plane. This allows for the direct generation of compositional shapes within a single tri-plane denoising diffusion process.

**Compositional 3D Reconstruction and Generation.** Researches on reconstructing [7, 29, 30, 32, 35] and generating [5, 18] holistic 3D scenes/objects have been widely investigated. For 3D reconstruction, ObjectSDF [29] and ObjectSDF++ [30] introduced an object-composition neural implicit representation, which allows for the individual reconstruction of every piece of furniture

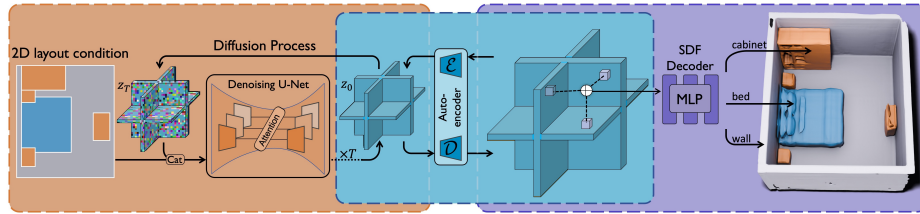


**Fig. 2:** Overview of Frankenstein. **Conditional denoising:** given a 2D semantic layout map, a diffusion model denoises the noise into a latent tri-plane. **VAE training:** a VAE then upsamples the latent tri-plane into higher resolution. **Tri-plane fitting:** a lightweight MLP finally decodes the high-resolution tri-plane into multiple semantic-wise SDFs.

in a room from image inputs; DELTA [7] introduced hybrid explicit-implicit 3D representations for the joint reconstruction of compositional avatars, such as the face and body, or hair and clothing, respectively. In the field of 3D generation, Po et al. [18] proposed a locally conditioned diffusion model, which can generate coherent compositional 3D scenes over semantic parts defined by text prompts and bounding boxes. Epstein et al. [5] jointly optimizes multiple NeRFs, each for a distinct object, along with layouts that combine these objects into scenes. In contrast to [5, 18], our method generates compositional 3D scenes in a single reverse diffusion process rather than relying on multiple time-consuming Score Distillation Sampling (SDS) optimizations.

**Room-scale Scene Synthesis.** Despite achieving impressive results in the synthesis of objects, the challenge of generating large and complex scenes persists. The main difficulties lie in the high variance of scene geometry and complex positional relationships between different scene elements. Object-retrieval-based approaches initially generate the room layout based on scene graphs [25, 28, 33] or auto-regressive transformer models [25], and then fill the layouts with objects that are searched from a given database. However, these methods either do not consider the wall, an important element in the room scene, or will produce unnecessary penetration caused by inappropriate object placement. Text2Room [13] utilized a pre-trained 2D inpainting model to generate RGBD images and then fused these images into 3D. Similarly, Ctrl-Room [6] lifted generated panorama images to 3D rooms, and they proposed a layout bounding boxes conditioned scene generation approach. The above 2D lifting-based approaches provide diverse contents but usually suffer from shape distortion. CC3D [1] used a conditional StyleGAN2 backbone to generate a 3D feature volume from a 2D semantic layout image and then used volume rendering to generate multi-view images of the room.

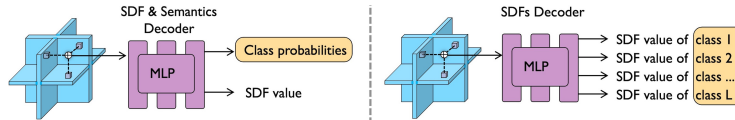


Fig. 3: Two approaches to incorporate semantic information into neural fields.

### 3 Method

This section provides details of our proposed framework (illustrated in Fig. 2) for the **room generation** task as an example. Sec. 3.1 introduces how we convert each 3D model into a tri-plane based implicit representation. Sec. 3.2 describes how we further encode tri-planes into a compact latent space. Sec. 3.3 presents how we realize controllable generation using diffusion models.

#### 3.1 Tri-Plane Fitting

Given a room  $\mathcal{R} = \{\mathcal{R}_1, \dots, \mathcal{R}_L\}$  with  $L$  classes of components, e.g., bed, cabinet, and wall, our goal is to train a tri-plane  $\mathbf{T} = \{\mathbf{T}_{xy}, \mathbf{T}_{xz}, \mathbf{T}_{yz}\} \in \mathbb{R}^{3 \times C \times R_h \times R_h}$  that can be decoded into  $L$  separate SDFs by an MLP  $\Phi$ , and each SDF represents a class of room element. The tri-plane  $\mathbf{T}$  is a spatial-aware tensor that can be queried by a 3D position  $\mathbf{p} \in \mathbb{R}^3$  and returns a feature vector  $\mathbf{f} \in \mathbb{R}^C$ :

$$\mathbf{f} = \text{Query}(\mathbf{T}, \mathbf{p}), \quad (1)$$

where the  $\text{Query}(\cdot)$  operation involves the summation of the 3 feature vectors that are bi-linearly sampled at  $\mathbf{p}$ 's projection coordinates on three planes  $\mathbf{T}_{xy}$ ,  $\mathbf{T}_{xz}$ , and  $\mathbf{T}_{yz}$ , respectively.

**Incorporating Semantics with Shapes.** In neural field-based 3D reconstruction, numerous methodologies [29, 30, 32, 35] for incorporating semantic information with 3D shapes have been investigated. Fig. 3 illustrates two ways, denoted as  $\mathcal{T}$  and  $\Phi$ , from left to right. Specifically,  $\mathcal{T}$  outputs a single SDF shape with a 3D semantic field

$$(d, \mathbf{h}) = \mathcal{T}(\mathbf{f}), \quad (2)$$

where  $\mathbf{f} \in \mathbb{R}^C$  is the feature vector queried from the tri-plane,  $d \in \mathbb{R}$  is the SDF value,  $\mathbf{h} \in \mathbb{R}^L$  is the one-hot vector indicating the class probability. Then the scene can be decomposed by grouping the points on the shape surface with their class labels. However this hard segmentation inevitably tear the surface of the shape and cause incompleteness in the decomposed parts. In contrast,  $\Phi$  directly produces multiple shapes with each representing a distinct class. It reads

$$(d_1, \dots, d_L) = \Phi(\mathbf{f}), \quad (3)$$

where  $d_i \in \mathbb{R}$  is the SDF value of the  $i$ -th class. We choose  $\Phi$  as our 3D representation because it retains complete shapes for each class. The output class-wise SDFs is denoted as  $\mathbf{D} = (d_1, \dots, d_L) \in \mathbb{R}^L$ .

**Training Point Sampling Strategy.** The ground truth room scene is pre-processed in a compositional format: i.e., each part of the room, e.g., wall and chair, is represented by a separate triangle mesh. We apply a semantic-aware on-surface point sampling strategy: given the mesh of the  $l$ -th class, we samples point set  $\mathbf{P}_l \in \mathbb{R}^{N_l \times 3}$  uniformly on the surface and compute the corresponding normal vectors as  $\mathbf{n}_l \in \mathbb{R}^{N_l \times 3}$ , then we obtain  $\{\mathbf{P}_1, \dots, \mathbf{P}_L, \mathbf{n}_1, \dots, \mathbf{n}_L\}$  by merging samples from all classes. We also sample off-surface points. For SDF values, we randomly sample points  $\mathbf{P}_{sdf} \in \mathbb{R}^{M \times 3}$  inside the  $[-1, 1]^3$  cubic, and compute the class-wise SDF values as  $\mathbf{D}_{sdf} \in \mathbb{R}^{M \times L}$ . Additionally, we randomly sample point set  $\mathbf{P}_{rnd} \in \mathbb{R}^{M \times 3}$  in  $[-1, 1]^3$  during every training epoch.

**Class-Specific Geometry Loss.** To learn a unified tri-plane feature space, the weight of MLP  $\Phi$  should be fixed for all training scenes. Therefore, we jointly optimize  $\Phi$  and the tri-planes of a subset of 10 rooms until convergence and then freeze  $\Phi$  to perform per-scene fitting for the rest of rooms in the dataset. The loss function is:

$$\mathcal{L}_{tri} = \lambda_1 \mathcal{L}_{eik} + \lambda_2 \mathcal{L}_{sdf} + \lambda_3 \mathcal{L}_{sur} + \lambda_4 \mathcal{L}_{nor} \quad (4)$$

The predicted SDF values  $\{\tilde{\mathbf{d}}_1 \in \mathbb{R}^{N_1}, \dots, \tilde{\mathbf{d}}_L \in \mathbb{R}^{N_L}, \tilde{\mathbf{D}}_{sdf} \in \mathbb{R}^{M \times L}\}$  and normal vectors  $\{\tilde{\mathbf{n}}_1 \in \mathbb{R}^{N_1 \times 3}, \dots, \tilde{\mathbf{n}}_L \in \mathbb{R}^{N_L \times 3}, \tilde{\mathbf{N}}_{rnd} \in \mathbb{R}^{M \times L \times 3}\}$  are obtained by applying  $\Phi(\mathbf{T}(\cdot))$  and  $\nabla\Phi(\mathbf{T}(\cdot))$  to all points in  $\{\mathbf{P}_1, \dots, \mathbf{P}_L, \mathbf{P}_{sdf}, \mathbf{P}_{rnd}\}$ , where the gradient  $\nabla$  is performed using finite difference to approximate the normal vector. Note that  $\tilde{\mathbf{d}}_{pcd}$  and  $\tilde{\mathbf{n}}_{pcd}$  remove the dimension for semantics, since the ground truth label is known for points in  $\mathbf{P}_{pcd}$ . Therefore the above terms are:

$$\mathcal{L}_{eik} = \frac{1}{ML} (\|\tilde{\mathbf{N}}_{rnd}\|_2 - 1)^2, \quad \mathcal{L}_{sdf} = \frac{1}{ML} \|\tilde{\mathbf{D}}_{sdf} - \mathbf{D}_{sdf}\|_1,$$

where  $\|\cdot\|_1$  denotes L1-norm, and  $\|\cdot\|_2$  denotes L2-norm. The following terms are calculated in a class-specific way

$$\mathcal{L}_{sur} = \sum_{l=1}^L \frac{1}{N_l} \|\tilde{\mathbf{d}}_l\|_1, \quad \mathcal{L}_{nor} = \frac{1}{L} \sum_{l=1}^L \frac{1}{N_l} \|\tilde{\mathbf{n}}_l - \mathbf{n}_l\|_2.$$

The above two terms alleviate the potential unbalanced point sampling, encouraging the reconstruction of semantic parts with small surface areas.

**Coarse-to-fine Optimization.** When calculating the surface normal vector using finite difference, discrete representations like tri-plane often face the gradient locality problem [15]. Specifically, the gradient computation involves only neighboring features within a small step, which prevents it from affecting the optimization of tri-plane features beyond the adjacent grids. We found that this could cause noisy shape-fitting results and typically requires a large number of

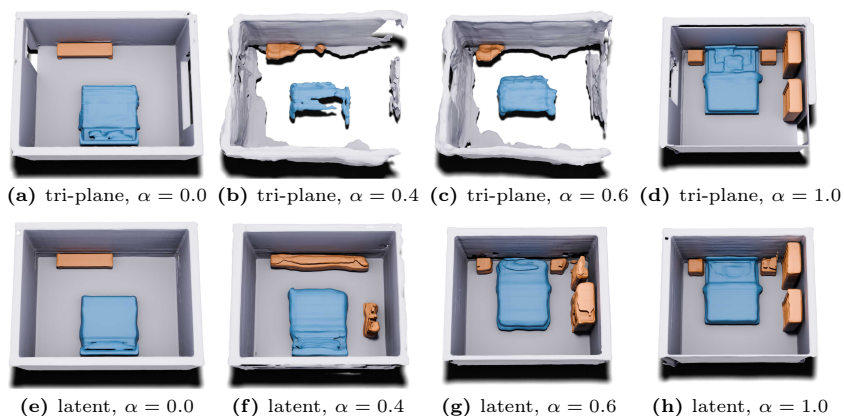


**Fig. 4:** Interpolation between two rooms on tri-plane space and latent tri-plane space.

training points. Neuralangelo [15] proposed to leverage the numerical gradient and progressive Level of Details (LoD) to address this problem. However, this approach requires a pyramid of 3D feature grids, and generating such a pyramid data structure with diffusion model is not trivial. In this paper, we fix the gradient locality problem with only one tri-plane. Specifically, we develop a coarse-to-fine training strategy to fit a single high-resolution tri-plane. First, we train a low-resolution tri-plane with  $R_l^2$  to delineate the approximate semantics and shape of the scene. Then, we upsample the tri-plane to  $(2R_l)^2$  using bi-linear interpolation and refine the features at the larger tri-plane. This process is repeated until the resolution reaches  $R_h^2 = 2^n R_l$ . We discover that this straightforward strategy is effective in reconstructing compositional 3D shapes.

### 3.2 VAE Training

Directly training diffusion model on the fitted tri-plane  $\mathbf{T} \in \mathbb{R}^{3 \times C \times R_h \times R_h}$  is impracticable due to the high computational cost (the sizes are  $R_h = 160$  and  $C = 32$ ). Additionally, the tri-plane space does not form a continuous distribution. For example, the interpolation between two tri-planes appears meaningless (See Fig. 4), which is not conducive to diffusion models. To this end, we follow BlockFusion [31] and employ an VAE to compress the tri-planes into a more compact and continuous latent space. The VAE performs the following mapping:

$$\mathcal{E} : \mathbb{R}^{3 \times C \times R_h \times R_h} \mapsto \mathbb{R}^{3 \times c \times r \times r}, \quad \mathcal{D} : \mathbb{R}^{3 \times c \times r \times r} \mapsto \mathbb{R}^{3 \times C \times R_h \times R_h}, \quad (5)$$

where  $\mathcal{E}$  is the encoder,  $\mathcal{D}$  is the decoder, and  $r < R_h$  is the latent plane size. VAE is trained with the following loss:

$$\mathcal{L}_{vae} = \lambda_{rec} \mathcal{L}_{rec} + \lambda_{KL} \mathcal{L}_{KL} + \lambda_{tri} \mathcal{L}_{tri}, \quad (6)$$

where  $\mathcal{L}_{rec}$  is the L1-loss between reconstructed tri-plane  $\tilde{\mathbf{T}} = \mathcal{D}(\mathcal{E}(\mathbf{T}))$  and the ground truth tri-plane  $\mathbf{T}$ ,  $\mathcal{L}_{KL}$  is the KL-divergence. Since the purpose is to learn a latent tri-plane that can faithfully represent the shape, we rely on  $\mathcal{L}_{tri}$  as the dominate loss during VAE training.  $\mathcal{L}_{tri}$  is computed similar as in Sec. 3.1, but using the queried features from the reconstructed tri-plane  $\tilde{\mathbf{T}}$ .

### 3.3 Conditional Denoising

A well-trained VAE defines a latent space that is capable of not only reconstructing relatively complete room-scale geometry but also generating reasonable results through random sampling. Conditional or unconditional diffusion model can be applied to this latent space for generation. In this section, we take layout-conditioned room generation for example.

For a room  $\mathcal{R}$  with  $L$  classes, the room layout is represented by the tensor  $\mathcal{F} \in \mathbb{R}^{L \times r \times r}$ , with each channel  $\mathcal{F}_i \in \mathbb{R}^{r \times r}$  as a binary map indicating whether or not an object class is placed.  $\mathcal{F}$  is computed by orthographically projecting room elements onto the floor plane. To condition on the floor layout, we follow [31] to directly concatenate the latent tri-plane and the floor layout as  $z_0 \in \mathbb{R}^{3 \times (c+L) \times r \times r}$ . Since the  $xz$  plane is aligned with the floor layout, we only concatenate  $\mathcal{F}$  into the  $xz$  plane of the latent tri-plane and pad the other planes with zeros:

$$z_0 = \{\hat{\mathbf{T}}_{xy} \oplus \mathbf{0}, \hat{\mathbf{T}}_{xz} \oplus \mathcal{F}, \hat{\mathbf{T}}_{yz} \oplus \mathbf{0}\}. \quad (7)$$

In every iteration, we sample a timestep  $t$  and add Gaussian noise  $\epsilon$  to obtain  $z_t$  from  $z_0$ :

$$z_t = \{\hat{\mathbf{T}}_{xy}^{noised} \oplus \mathbf{0}, \hat{\mathbf{T}}_{xz}^{noised} \oplus \mathcal{F}, \hat{\mathbf{T}}_{yz}^{noised} \oplus \mathbf{0}\}. \quad (8)$$

And we train a U-Net shaped denoising backbone  $\Psi$  to recover the latent tri-plane. Instead of predicting the noise  $\epsilon$  as in the original DDPM [12], we predict  $z_0$  in our task. The loss function reads:

$$\mathcal{L}_{diff} = \|\Psi(z_t, \gamma(t)) - z_0\|_2^2, \quad (9)$$

where  $\gamma(\cdot)$  is a positional encoding function and  $\|\cdot\|_2^2$  is MSE loss.

## 4 Experiments

**Dataset.** Our room-scale scenes dataset is obtained from 3D-FRONT [8] and 3D-FUTURE [9]. The following pre-processes are performed: 1) The raw meshes are transformed into watertight ones using Blender’s *voxel remeshing* tool. 2) The positions of the furniture are adjusted if penetration is detected. This resolves the collision problem and provides a physically plausible training scene. The final dataset contains 2558 bedrooms with 3 classes {wall, bed, cabinet}. For VAE training, the fitted tri-planes are augmented by 8 times via rotations and flips.



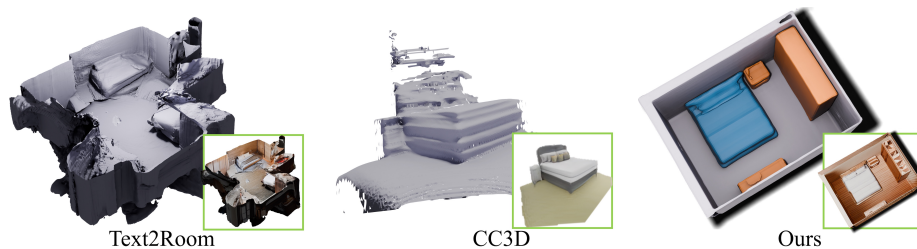


**Fig. 5: Qualitative room generation results.** The prompt for Text2Room [13] is “a wooden style bedroom with a king-size bed and large wardrobes.” The textures of ours are generated using Text2Tex [2] based on prompt “wooden”. The geometry of CC3D [1] is reconstructed from a point cloud extracted from depth images using ball-pivoting.

**Implementation Details.** The hyper-parameters are empirically set to  $L = 3$ ,  $C = 32$ ,  $R_h = 160$ ,  $R_l = 5$ ,  $M = 300000$ ,  $c = 4$ ,  $r = 40$ . For tri-plane fitting, we weigh the individual losses with  $\lambda_1 = 0.2$ ,  $\lambda_2 = 10.0$ ,  $\lambda_3 = 10.0$ ,  $\lambda_4 = 0.5$ , and equally sample  $N_1 = N_2 = N_3 = 100000$  points for each category. For VAE training, we instead sample  $N_1 = 20000$ ,  $N_2 = N_3 = 5000$  points and set  $\lambda_{rec} = 0.1$ ,  $\lambda_{KL} = 1.0$ ,  $\lambda_{tri} = 1.0$ . Channel-wise normalization [23] is applied to the (latent) tri-plane features during VAE and diffusion training (Sec. 4.3 shows ablation study of normalization strategy). We run tri-plane fitting on multiple NVIDIA T10 GPUs, and the other stages on 8 NVIDIA V100 GPUs. We assess the reconstruction quality using Chamfer Distance (CD).

#### 4.1 Compositional Room Generation

We compare with two room generation baselines, Text2Room [13] and CC3D [1]. CC3D [1] also enables layout control. Fig. 5 shows the qualitative results. Overall our model produces superior room geometry than Text2Room and more plausible layouts than CC3D. Fig. 6 displays various applications applied to our generated meshes. Semantic-compositional scenes provide semantic priors, which are compatible with off-the-shelf object-targeted texturing models. We utilize [2] to texture individual scene components in four styles. Additionally, object rearrangements can be performed to customize the room layout and appearance. Moreover, retrieval and refinement can be implemented as a post-processing stage to further enhance the quality of 3D models.

#### 4.2 Compositional Avatar Generation

In addition to room scenes, we also demonstrate the capacity of Frankenstein for compositional avatar generation. In this experiment, Frankenstein is trained and tested on a dataset of around 10K cartoon avatars from Vroid [3], with each avatar being decomposed into body, clothing, and hair parts. These avatar scenes pose a bigger challenge than the room scenes, as the level of shape entanglement



Fig. 6: Applications of semantic-compositional room generation.

between two parts of an avatar, e.g., hair and body, is much higher than that in room furniture and walls. Nonetheless, Frankenstein still manages to successfully generate clean and separable shapes. As shown in Fig. 7, the generated compositional avatar facilitates numerous downstream applications, including component-wise texture generation, random cloth swapping, cloth re-targeting, and automatic rigging and animation. The hair and clothing textures are generated using [2]. Cloth re-targeting is done by first registering the source and target bodies with a SMPLX [17] model and then transforming the cloth based on a dense warping field computed between two SMPLX bodies; this procedure follows Delta [7].

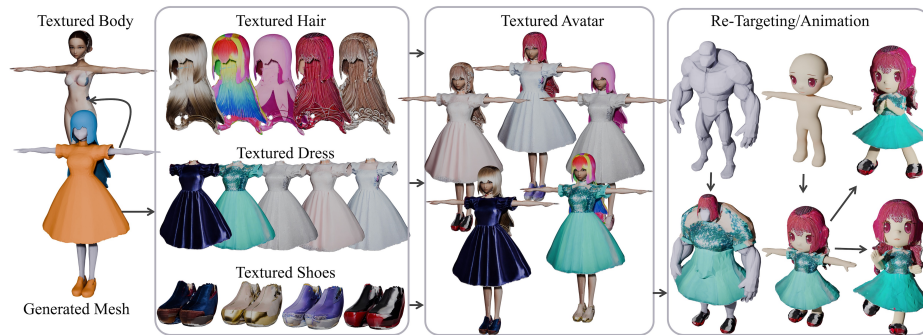
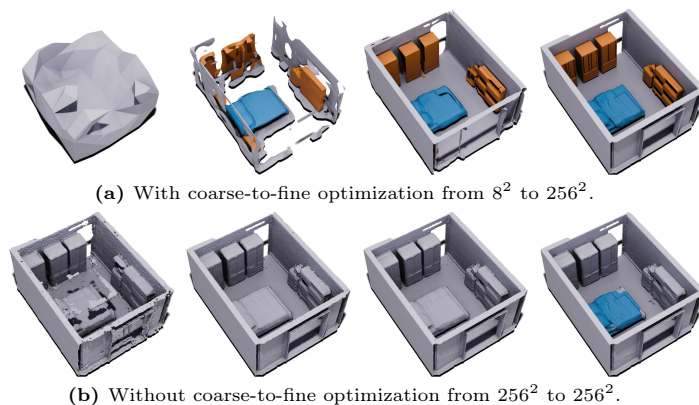


Fig. 7: Applications of semantic-compositional avatar generation.



**Fig. 8:** Visualization of the whole room (wall, bed, cabinet) during tri-plane fitting with or without coarse-to-fine optimization.

### 4.3 Ablation Study

**Is coarse-to-fine optimization necessary?** Fig. 8 illustrates the reconstructed rooms during tri-plane fitting, with and without coarse-to-fine optimization. Optimizing tri-planes directly at high resolution fails to correct misclassified meshes that appear in the early training stage due to the gradient locality issue. By starting at a low resolution, the room’s approximate semantics and shape can be outlined and subsequently refined smoothly at higher resolutions. Tab. 1 quantitatively proves the necessity. Additionally, coarse-to-fine optimization reduces the fitting time from 380s to 279s over 500 iterations.

**Ablation of tri-plane fitting.** Tab. 1 and Fig. 9 show an ablation study for tri-plane fitting with different point sampling and optimization strategies. We control the following 3 configurations with different combinations: **C2F** indicates using coarse-to-fine optimization; **SSS** indicates using semantic-aware sampling strategy that samples points uniformly for each category ( $N_1 \approx N_2 \approx N_3$ ) rather than uniformly on the entire room ( $N_1 \gg N_2, N_1 \gg N_3$ ); **SNS** indicates sampling  $\mathbf{P}_{sdf}$  on both  $[-1, 1]^3$  cubic space and space near surface rather than only on  $[-1, 1]^3$ . The {C2F,SSS,SNS} combination demonstrates that coarse-to-fine optimization alone is insufficient to resolve semantic coupling, i.e., a bed may appear within a wall. Of the four terms in  $\mathcal{L}_{tri}$ , only  $\mathcal{L}_{sdf}$  contributes to semantic isolation, which leaves room for the risk of semantic coupling. Since semantic coupling often manifests as the reflection of one category’s surface in another, the comparison between {C2F,SSS,SNS} and {C2F,SSS,SNS} proves that the additional ground truth SDF values near objects can alleviate this issue. {C2F,SSS,SNS} slightly outperforms {C2F,SSS,SNS} due to more sampled points on the wall under fitting task. We will highlight the importance of SSS in VAE training later.

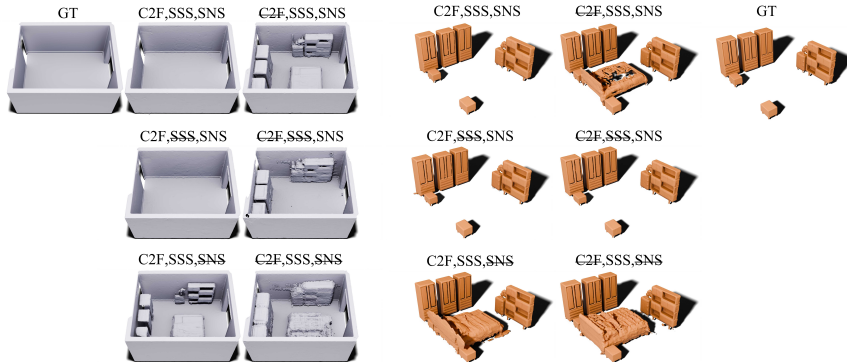


**Fig. 9: Ablation studies on tri-plane fitting.** As the generated beds are nearly the same in all experiments, we only show the results of wall and cabinet.

**Table 1: Ablation studies on tri-plane fitting.** CDs are computed for each semantic group.

C2F	SSS	SNS	$\mathcal{L}_{eik} \times 10^{-2}$	$\mathcal{L}_{sdf} \times 10^{-2}$	$CD_{wall} \times 10^{-3}$	$CD_{bed} \times 10^{-3}$	$CD_{cabinet} \times 10^{-3}$
✓	✓	✓	4.33	1.01	0.94	<b>0.11</b>	<b>0.26</b>
	✓	✓	14.44	3.79	2.00	0.14	6.81
✓		✓	<b>2.32</b>	<b>0.31</b>	<b>0.89</b>	<b>0.11</b>	<b>0.26</b>
		✓	9.50	2.09	1.58	0.14	0.27
✓	✓		6.20	0.55	1.67	<b>0.11</b>	8.74
	✓		9.17	1.28	2.25	0.13	8.62

**Dimensions of the latent tri-plane.** Tab. 2 presents the quantitative results of varying hyper-parameters on a small dataset (720 training rooms and 80 testing rooms) after 5k iterations. We explore different latent resolutions of  $r = 20, 40, 80$  and channel dimensions of  $c = 1, 4, 8$ . The latent’s dimension greatly affects the generation results: a higher latent resolution leads to improved performance. While resolution with  $80 \times 80$  imposes a significant computational overhead, we regard  $40 \times 40$  as a good trade-off between efficiency and quality. In the experiments on channel dimensions, we find that increasing number of channels lead to more complete wall shape. To balance efficiency and the geometry quality, we set  $c = 4$ .

**Table 2: Ablation Studies on VAE.** CDs are computed for wall/bed/cabinet.

Dim	(4,20,20)	(1,40,40)	(4,40,40)	(8,40,40)	(4,80,80)
$CD(\text{train}) \times 10^{-3}$	5.31/0.96/1.20	3.82/0.72/1.36	3.15/ <b>0.52/0.94</b>	<b>1.81</b> /0.58/1.33	<b>1.45/0.23/0.40</b>
$CD(\text{test}) \times 10^{-3}$	6.04/1.52/2.06	3.72/1.54/4.00	4.02/ <b>1.24/1.83</b>	<b>3.08</b> /1.32/2.09	<b>2.30/0.83/1.00</b>
Speed(s/iter)	18	21	21	22	34

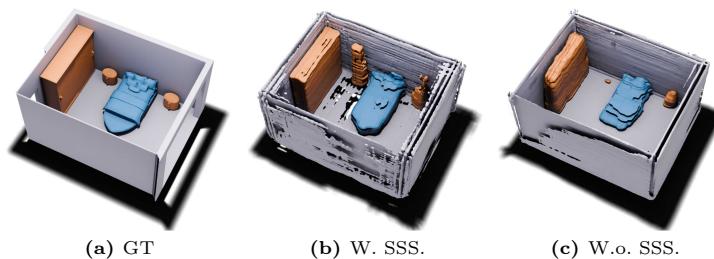


**Fig. 10:** Qualitative results on the semantic-aware sampling strategy (SSS).

**Is the semantic-aware sampling strategy necessary?** Fig. 10 and Tab. 3 demonstrate that the model has difficulty recovering the details of furniture without semantic-aware sampling strategy (SSS). The model is trained on a small dataset (720 training rooms and 80 testing rooms) for 5k iterations. Since walls dominate in terms of surface area compared to furniture, when we uniformly sample points across the entire mesh, most points are from walls, resulting in incomplete furniture (see Fig. 10c). To address this, we sample  $N_1 : N_2 : N_3 = 4 : 1 : 1$  to achieve a relatively balanced sampling across classes and calculate the loss function separately for each class. The results exhibit improved furniture details but rougher walls (see Fig. 10b). We opt to apply SSS to enhance the details of the furniture.

**Table 3:** Quantitative results on the semantic-aware sampling strategy (SSS). CDs are computed for wall/bed/cabinet.

Model	$ \text{CD}(\text{train}) \times 10^{-3} $	$ \text{CD}(\text{test}) \times 10^{-3} $
w. SSS	3.15/ <b>0.52</b> / <b>0.94</b>	4.02/ <b>1.24</b> / <b>1.83</b>
w.o. SSS	<b>2.78</b> /1.03/14.48	<b>3.23</b> /1.83/8.59

**How does the normalization effect the diffusion model?** Scale normalization maintains the standard deviation of the data close to 1.0 by multiplying a scale coefficient [21]. However, this approach is not effective for our task as it only generates walls of poor quality. We hypothesize that the wall feature dominates most of the  $C$  channels, and other semantics may be overlooked if multiplied by a relatively large coefficient. With channel-wise normalization, all semantics can be effectively generated (see Fig. 11). The model is trained on a small dataset ( $\approx 2k$  latent tri-planes).

**Is Frankenstein generalizable?** Fig. 12 presents room generation results conditioned on various layout maps. Our model demonstrates the ability to adhere

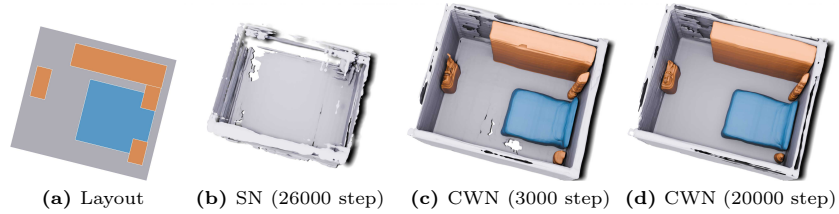


**Fig. 11:** Scale normalization (SN) v.s. channel-wise normalization (CWN).

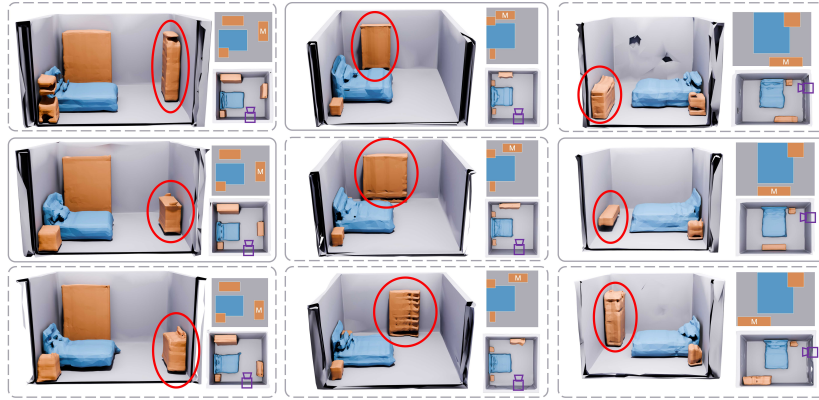


**Fig. 12:** Qualitative results of layout-conditioned room generation. The layout maps in solid line are from the training dataset, and the other two layout maps in the same column are generated by translating one of the furniture (marked as “M”).

to a conditional layout while maintaining generation capacity when altering the layouts configuration. We randomly select three layout maps from the training dataset and translate one of the objects along the wall, resulting in new layouts that remain reasonable. It is important to note that these new layouts do not exist in the training set. Conditioned on these new layouts, Frankenstein successfully generates corresponding 3D rooms that are reasonable. This showcases the model’s generalization capacity.

## 5 Conclusion

In summary, we develop Frankenstein, an innovative tri-plane diffusion-based method that is capable of generating semantic-compositional 3D scenes. We extend the tri-plane tensor factorization to represent compositional shapes by decoding multiple SDFs from a single tri-plane, each of which represents the shape of a distinct semantic class. This novel representation permits the concurrent modelling of multiple comprehensive shapes within a single tri-plane tensor, ensuring distinct scene separation and a diverse range of generated shapes. The generated scenes offer a range of customized controls, including but not

limited to, component-wise texturing, rearrangement of room objects, and the re-targeting of avatar clothing and hair.

**Limitations.** The current implementation of Frankenstein faces several limitations. 1) Given that our method utilizes only a single tri-plane to model the entire scene, the details are limited by the resolution. One potential solution could involve combining our approach with [31], which divides large scenes into multiple smaller blocks. 2) The training process for the VAE is slow ( $\approx$  a week), incorporating more efficient backbone is a future direction. 3) While our method demonstrates generalizability in layout conditions, it still exhibits some flaws (e.g. holes in the wall in Fig. 12) with layouts beyond the dataset. We believe that these issues can be mitigated through the use of additional training data.

## References

1. Bahmani, S., Park, J.J., Paschalidou, D., Yan, X., Wetzstein, G., Guibas, L., Tagliasacchi, A.: Cc3d: Layout-conditioned generation of compositional 3d scenes. arXiv:2303.12074 (2023)
2. Chen, D.Z., Siddiqui, Y., Lee, H.Y., Tulyakov, S., Nießner, M.: Text2tex: Text-driven texture synthesis via diffusion models. arXiv:2303.11396 (2023)
3. Chen, S., Zhang, K., Shi, Y., Wang, H., Zhu, Y., Song, G., An, S., Kristjansson, J., Yang, X., Zwicker, M.: Panic-3d: Stylized single-view 3d reconstruction from portraits of anime characters. In: CVPR (2023)
4. Chou, G., Bahat, Y., Heide, F.: Diffusion-sdf: Conditional generative modeling of signed distance functions. In: ICCV (2023)
5. Epstein, D., Poole, B., Mildenhall, B., Efros, A.A., Holynski, A.: Disentangled 3d scene generation with layout learning. arXiv:2402.16936 (2024)
6. Fang, C., Hu, X., Luo, K., Tan, P.: Ctrl-room: Controllable text-to-3d room meshes generation with layout constraints. arXiv:2310.03602 (2023)
7. Feng, Y., Liu, W., Bolkart, T., Yang, J., Pollefeys, M., Black, M.J.: Learning disentangled avatars with hybrid 3d representations. arXiv:2309.06441 (2023)
8. Fu, H., Cai, B., Gao, L., Zhang, L.X., Wang, J., Li, C., Zeng, Q., Sun, C., Jia, R., Zhao, B., et al.: 3d-front: 3d furnished rooms with layouts and semantics. In: ICCV (2021)
9. Fu, H., Jia, R., Gao, L., Gong, M., Zhao, B., Maybank, S., Tao, D.: 3d-future: 3d furniture shape with texture. IJCV (2021)
10. Gao, J., Shen, T., Wang, Z., Chen, W., Yin, K., Li, D., Litany, O., Gojcic, Z., Fidler, S.: Get3d: A generative model of high quality 3d textured shapes learned from images. In: NeurIPS (2022)
11. Gupta, A., Xiong, W., Nie, Y., Jones, I., Oğuz, B.: 3dgen: Triplane latent diffusion for textured mesh generation. arXiv:2303.05371 (2023)
12. Ho, J., Jain, A., Abbeel, P.: Denoising diffusion probabilistic models. In: NeurIPS (2020)
13. Höllein, L., Cao, A., Owens, A., Johnson, J., Nießner, M.: Text2room: Extracting textured 3d meshes from 2d text-to-image models. arXiv:2303.11989 (2023)
14. Hong, Y., Zhang, K., Gu, J., Bi, S., Zhou, Y., Liu, D., Liu, F., Sunkavalli, K., Bui, T., Tan, H.: Lrm: Large reconstruction model for single image to 3d. arXiv:2311.04400 (2023)

15. Li, Z., Müller, T., Evans, A., Taylor, R.H., Unberath, M., Liu, M.Y., Lin, C.H.: Neuralangelo: High-fidelity neural surface reconstruction. In: CVPR (2023)
16. Mildenhall, B., Srinivasan, P.P., Tancik, M., Barron, J.T., Ramamoorthi, R., Ng, R.: Nerf: Representing scenes as neural radiance fields for view synthesis. In: ECCV (2020)
17. Pavlakos, G., Choutas, V., Ghorbani, N., Bolkart, T., Osman, A.A.A., Tzionas, D., Black, M.J.: Expressive body capture: 3D hands, face, and body from a single image. In: CVPR (2019)
18. Po, R., Wetzstein, G.: Compositional 3d scene generation using locally conditioned diffusion. arXiv:2303.12218 (2023)
19. Poole, B., Jain, A., Barron, J.T., Mildenhall, B.: Dreamfusion: Text-to-3d using 2d diffusion. arXiv:2209.14988 (2022)
20. Qian, G., Mai, J., Hamdi, A., Ren, J., Siarohin, A., Li, B., Lee, H.Y., Skorokhodov, I., Wonka, P., Tulyakov, S., et al.: Magic123: One image to high-quality 3d object generation using both 2d and 3d diffusion priors. arXiv:2306.17843 (2023)
21. Rombach, R., Blattmann, A., Lorenz, D., Esser, P., Ommer, B.: High-resolution image synthesis with latent diffusion models. In: CVPR (2022)
22. Shi, R., Chen, H., Zhang, Z., Liu, M., Xu, C., Wei, X., Chen, L., Zeng, C., Su, H.: Zero123++: a single image to consistent multi-view diffusion base model. arXiv:2310.15110 (2023)
23. Shue, J.R., Chan, E.R., Po, R., Ankner, Z., Wu, J., Wetzstein, G.: 3d neural field generation using triplane diffusion. In: CVPR (2023)
24. Sohl-Dickstein, J., Weiss, E., Maheswaranathan, N., Ganguli, S.: Deep unsupervised learning using nonequilibrium thermodynamics. In: ICML (2015)
25. Tang, J., Nie, Y., Markhasin, L., Dai, A., Thies, J., Nießner, M.: Diffuscene: Scene graph denoising diffusion probabilistic model for generative indoor scene synthesis. arXiv:2303.14207 (2023)
26. Vaswani, A., Shazeer, N., Parmar, N., Uszkoreit, J., Jones, L., Gomez, A.N., Kaiser, Ł., Polosukhin, I.: Attention is all you need. In: NeurIPS (2017)
27. Wang, T., Zhang, B., Zhang, T., Gu, S., Bao, J., Baltrusaitis, T., Shen, J., Chen, D., Wen, F., Chen, Q., et al.: Rodin: A generative model for sculpting 3d digital avatars using diffusion. In: CVPR (2023)
28. Wen, Z., Liu, Z., Sridhar, S., Fu, R.: Anyhome: Open-vocabulary generation of structured and textured 3d homes. arXiv:2312.06644 (2023)
29. Wu, Q., Liu, X., Chen, Y., Li, K., Zheng, C., Cai, J., Zheng, J.: Object-compositional neural implicit surfaces. In: ECCV (2022)
30. Wu, Q., Wang, K., Li, K., Zheng, J., Cai, J.: Objectsdf++: Improved object-compositional neural implicit surfaces. In: ICCV (2023)
31. Wu, Z., Li, Y., Yan, H., Shang, T., Sun, W., Wang, S., Cui, R., Liu, W., Sato, H., Li, H., Ji, P.: Blockfusion: Expandable 3d scene generation using latent tri-plane extrapolation. arXiv:2401.17053 (2024)
32. Yang, B., Zhang, Y., Xu, Y., Li, Y., Zhou, H., Bao, H., Zhang, G., Cui, Z.: Learning object-compositional neural radiance field for editable scene rendering. In: ICCV (2021)
33. Zhai, G., Örnek, E.P., Wu, S.C., Di, Y., Tombari, F., Navab, N., Busam, B.: Commonsences: Generating commonsense 3d indoor scenes with scene graphs. arXiv:2305.16283 (2023)
34. Zheng, X.Y., Pan, H., Wang, P.S., Tong, X., Liu, Y., Shum, H.Y.: Locally attentional sdf diffusion for controllable 3d shape generation. arXiv:2305.04461 (2023)
35. Zhi, S., Laidlow, T., Leutenegger, S., Davison, A.J.: In-place scene labelling and understanding with implicit scene representation. In: ICCV (2021)